

# Near-field energy transfer between graphene and magneto-optic media

Gaomin Tang,<sup>1,\*</sup> Lei Zhang,<sup>2,3</sup> Yong Zhang,<sup>4,5</sup> Jun Chen,<sup>6,†</sup> and Che Ting Chan<sup>7</sup>

<sup>1</sup>*Department of Physics, University of Basel, Klingelbergstrasse 82, CH-4056 Basel, Switzerland*

<sup>2</sup>*State Key Laboratory of Quantum Optics and Quantum Optics Devices,  
Institute of Laser Spectroscopy, Shanxi University, Taiyuan 030006, China*

<sup>3</sup>*Collaborative Innovation Center of Extreme Optics, Shanxi University, Taiyuan 030006, China*

<sup>4</sup>*School of Energy Science and Engineering, Harbin Institute of Technology, Harbin 150001, P. R. China*

<sup>5</sup>*Key Laboratory of Aerospace Thermophysics, Ministry of Industry and Information Technology, Harbin 150001, P. R. China*

<sup>6</sup>*State Key Laboratory of Quantum Optics and Quantum Optics Devices,  
Institute of Theoretical Physics, Shanxi University, Taiyuan 030006, China*

<sup>7</sup>*Department of Physics and Institute for Advanced Study,  
The Hong Kong University of Science and Technology, Hong Kong, China*

Energy can be transferred in a radiative manner between objects with different electrical fluctuations. In this work, we consider near-field energy transfer between two separated parallel plates: one is graphene-covered boron nitride and the other a magneto-optic medium. We first study the energy transfer between the two plates having the same temperature. An electric current through the graphene gives rise to nonequilibrium fluctuations and induces the energy transfer. Both the magnitude and direction of the energy flux can be controlled by the electric current and an in-plane magnetic field in the magneto-optic medium. This is due to the interplay between nonreciprocal effective photonic temperature in graphene and nonreciprocal surface modes in the magneto-optic plate. Furthermore, we report that a tunable thermoelectric current can be generated in the graphene in the presence of a temperature difference between the two plates.

*Introduction.*— Nonreciprocity is attracting substantial interest in plasmonics and radiative energy harvesting. In magneto-optic materials, magnetic field breaks time-reversal symmetry which results in nonreciprocal electromagnetic surface waves. Thanks to the broken reciprocity, various novel phenomena of near-field heat transfer have been reported including photon thermal Hall effect [1], persistent heat current [2, 3], thermal magnetoresistance [4–7], thermal rectification [8], and thermal radiation-induced lateral Casimir force [9, 10].

In graphene, nonreciprocal surface plasmons can be generated by applying an electric current [11–15]. Interesting properties like negative Landau damping [16] and Fizeau drag [17, 18] have been studied. The current-biased graphene is in a nonequilibrium state, and this leads to a finite photonic chemical potential [19] that depends on wave vector  $\mathbf{q}$ . The Bose-Einstein distribution of photons at angular frequency  $\omega$  and temperature  $T$  becomes  $n(\omega) = [e^{\hbar(\omega - \mathbf{q} \cdot \mathbf{v}_d)/k_B T} - 1]^{-1}$  where  $\mathbf{v}_d$  is drift velocity of the electric current [20–23]. Thus, the effective photonic temperature  $T_{\text{eff}} = T\omega/(\omega - \mathbf{q} \cdot \mathbf{v}_d)$  can be nonreciprocal, i.e., different for  $\mathbf{q}$  and  $-\mathbf{q}$ . Regarding regulating photonic chemical potential, it has been reported that a p-n junction with a voltage bias [24] enables solid-state cooling in near-field regime [25–27].

In this Letter, we study the near-field energy transfer between two parallel plates: one is graphene-covered hexagonal boron nitride (GhBN) and the other magneto-optic medium [see Fig. 1(a)]. By applying an electric current through the graphene, there is a net energy transfer between the plates having an equal temperature. An in-plane magnetic field, which is perpendicular to the electric current, is applied to the magneto-optic medium. In the absence of the magnetic field, the energy flux flows from the GhBN to the magneto-optic medium in the absence of a temperature difference. Re-

markably, direction of the energy flux can be controlled by the magnetic field due to the nonreciprocal surface modes of the magneto-optic medium. Furthermore, a tunable thermoelectric current can be generated in graphene with a temperature difference between the two plates.

*Formalism.*— Within the framework of fluctuational electrodynamics [28, 29], the radiative energy flux  $H$  between two parallel plates across an air gap  $d$  is expressed as [29–37]

$$H = \int_0^\infty \frac{d\omega}{2\pi} \int \frac{d^2\mathbf{q}}{4\pi^2} \hbar\omega \delta n(\omega, q_x v_d) \xi(\omega, \mathbf{q}, B, d), \quad (1)$$

with  $\mathbf{q} = (q_x, q_y)$  the in-plane wave vector and  $\omega$  the angular frequency. By applying an electric current through the graphene which is characterized by drift velocity  $v_d$ , the difference of Bose-Einstein distributions from the two plates is [20–23]

$$\delta n(\omega, q_x v_d) = [e^{\hbar(\omega - q_x v_d)/k_B T_1} - 1]^{-1} - [e^{\hbar\omega/k_B T_2} - 1]^{-1}. \quad (2)$$

Here,  $T_1$  and  $T_2$  are temperatures of the two plates, respectively. The possible joule heating in graphene by the electric current has been considered in temperature  $T_1$  [17, 18]. The subscript “1” is used to denote the GhBN and “2” the magneto-optic medium. Without losing generality, the drift velocity  $v_d$  in graphene is assumed to be along the positive direction of the  $x$  axis. Equation (2) indicates that the electric current-induced nonequilibrium fluctuations result in a finite energy flux even in the absence of a temperature difference, i.e.,  $T_1 = T_2$ . The photonic transmission coefficient  $\xi(\omega, \mathbf{q}, B, d)$  with air-gap separation  $d$  and magnetic field  $B$  is expressed as

$$\xi = \begin{cases} \text{Tr}[(I - R_2^\dagger R_2)D(I - R_1 R_1^\dagger)D^\dagger], & q < k_0 \\ \text{Tr}[(R_2^\dagger - R_2)D(R_1 - R_1^\dagger)D^\dagger] e^{-2|\beta_0|d}, & q > k_0 \end{cases} \quad (3)$$

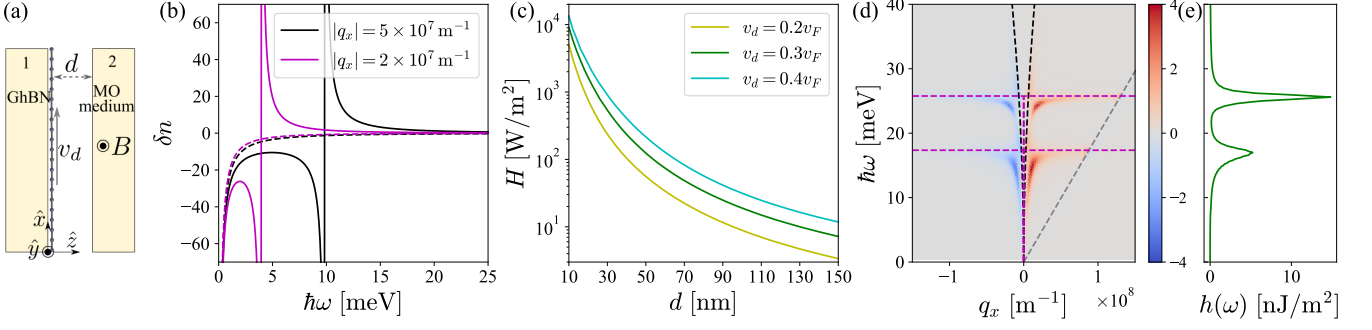


FIG. 1. (a) Schematic plot of the near-field energy transfer between two parallel plates with air gap  $d$ . The plates are, respectively, made of graphene-covered hexagonal boron nitride (GhBN) and magneto-optic (MO) medium. By applying an electric current with drift velocity  $v_d$  through the graphene, a net energy flux is transferred between the plates. Its magnitude and direction can be modulated by the electric current and the magnetic field  $B$  applied to the magneto-optic medium. (b)  $\delta n(\omega, q_x v_d)$  versus  $\hbar\omega$  at  $T_1 = T_2 = 300$  K and  $v_d = 0.3v_F$  with  $v_F = 10^6$  m/s. The solid and dashed lines are, respectively, for positive and negative  $q_x$ . (c) Energy flux  $H$  versus  $d$  at  $B = 0$  and different  $v_d$  with  $T_1 = T_2 = 300$  K. The magneto-optic medium is chosen as InSb. (d) Energy transmission  $\mathcal{Z}$  (in units of meV) at  $v_d = 0.3v_F$ ,  $d = 10$  nm, and  $q_y = 0$  is shown against  $q_x$  and  $\hbar\omega$ . The gray dashed line is  $\omega = q_x v_d$ . The black and magenta dashed lines are, respectively, the dispersion of surface modes of GhBN and InSb at  $B = 0$  without considering the damping. (e) Spectrum  $h(\omega)$  at  $v_d = 0.3v_F$  and  $d = 10$  nm. The vertical axes in (d) and (e) are the same.

where  $D = (I - R_1 R_2 e^{2i\beta_0 d})^{-1}$  and  $I$  is the identity matrix. The magnitude of the out-of-plane wave vector in air is  $\beta_0 = \sqrt{k_0^2 - q^2}$  with  $k_0 = \omega/c$  and  $q = |\mathbf{q}|$ . The reflection-coefficient matrix  $R_n$  at the surface of plate  $n$  with  $n = 1, 2$  is provided in the Supplemental Material [38]. The near- and far-field regions are delimited by  $q > k_0$  and  $q < k_0$ , respectively. From Eqs. (1) and (2), a positive energy flux  $H$  indicates that it flows from the GhBN plate to the magneto-optic plate and inversely for a negative flux. We define the energy transmission function as

$$\mathcal{Z}(\omega, \mathbf{q}, v_d, B) = \hbar\omega \delta n(\omega, q_x v_d) \xi(\omega, \mathbf{q}, B, d), \quad (4)$$

which gives the energy transfer at given  $\omega$  and  $\mathbf{q}$ . The spectrum  $h(\omega)$  of energy flux is defined through  $H = \int_0^\infty \frac{d\omega}{2\pi} h(\omega)$ .

The surface modes of a magneto-optic material are nonreciprocal in the Voigt configuration. To study the interplay of the nonreciprocal effects from the effective photonic temperature and the surface modes, the in-plane magnetic field is applied along the  $y$  direction. The dielectric tensor of the magneto-optic medium reads

$$\bar{\bar{\epsilon}}_{\text{MO}}(\omega) = \begin{bmatrix} \epsilon_d & 0 & i\epsilon_a \\ 0 & \epsilon_p & 0 \\ -i\epsilon_a & 0 & \epsilon_d \end{bmatrix}, \quad (5)$$

with  $\epsilon_a \propto B$ . The dispersion relation for  $p$ -polarized surface modes in the Voigt configuration is [39]

$$\epsilon_v \sqrt{k_0^2 - q_x^2} + \sqrt{\epsilon_v k_0^2 - q_x^2} - i\epsilon_a q_x / \epsilon_d = 0, \quad (6)$$

with  $\epsilon_v = \epsilon_d - \epsilon_a^2 / \epsilon_d$ . It can be seen that  $\epsilon_a$  gives rise to the nonreciprocal dispersion.

In magnetic Weyl semimetals, Weyl nodes separation in momentum space leads to anomalous Hall effect [40–42] so

that there are off-diagonal components in the dielectric tensor. Compared to the magneto-optic materials, magnetic Weyl semimetals support nonreciprocal surface polaritons intrinsically [43, 44]. Therefore, one can replace the magneto-optic medium by a magnetic Weyl semimetal so that an external magnetic field is no longer needed [7, 45–48].

Before exploring the energy transfer in detail, we discuss the properties of  $\delta n(\omega, q_x v_d)$  shown in Fig. 1(b) at  $T_1 = T_2 \equiv T = 300$  K and  $v_d = 0.3v_F$ . The solid and dashed lines are, respectively, for positive and negative  $q_x$ . For positive  $q_x$ ,  $\delta n$  is positive under  $\omega > q_x v_d$ , which means that the effective photonic temperature in the graphene  $T_{\text{eff}}$  is higher than  $T$ . Under  $\omega < q_x v_d$ , both the effective temperature and the real part of the graphene conductivity are negative [38]. This leads to the optical gain that the graphene plasmons absorb energy from the electric current [16]. In this work, we consider the gap separation  $d$  not less than 10 nm so that the contribution from  $\omega < q_x v_d$ , which is only sizable with a subnanometer separation [21, 22], can be neglected. Thus, the energy transfer is from the GhBN to the magneto-optic medium for positive  $q_x$ . For negative  $q_x$ ,  $\delta n$  is negative and the effective photonic temperature is lower than  $T$  so that the energy-transfer direction is opposite to that of positive  $q_x$ .

During the numerical calculation, we set the chemical potential of the graphene as 0.1 eV. The drift velocity in the graphene is set around  $0.3v_F$  so that the nonreciprocity of the plasmon dispersion can be neglected [11, 15]. This can be seen from the black dashed lines in Fig. 1(d). The magneto-optic medium is chosen to be InSb. The calculation details are provided in the Supplemental Material [38]. Below, we discuss the scenarios in the absence and presence of the magnetic fields separately with  $T_1 = T_2 = 300$  K.

*Energy transfer at  $B=0$ .*—Figure 1(c) shows the energy flux versus the gap separation  $d$  in the absence of a magnetic field.

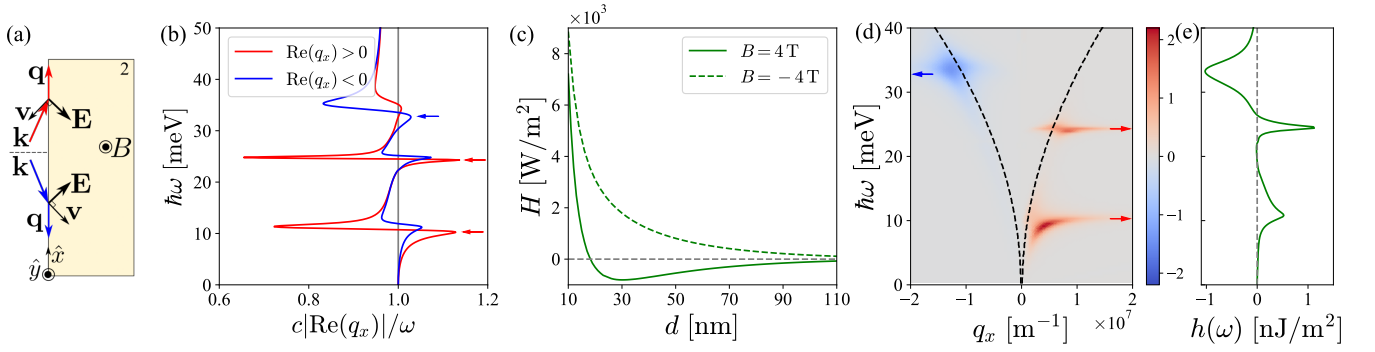


FIG. 2. (a) Schematic explanation for the nonreciprocal surface polaritons of magneto-optic medium where  $\mathbf{k}$  denotes wave vectors of incident electromagnetic fields from the free space. (b) Dispersion of the surface modes of InSb in the Voigt configuration at  $B = 4$  T. (c) Energy flux  $H$  versus separation  $d$  at  $B = 4$  T and  $B = -4$  T with  $v_d = 0.3v_F$ . Here,  $T_1 = T_2 = 300$  K. (d) The energy transmission function  $\mathcal{Z}$  (in units of meV) at  $B = 4$  T,  $d = 50$  nm, and  $q_y = 0$  is shown against  $q_x$  and  $\hbar\omega$ . The black dashed lines are the surface plasmon dispersions of the GhBN. The energies  $\hbar\omega$  indicated by the arrows are the same as the corresponding ones indicated in (b). (e) Spectrum  $h(\omega)$  at  $B = 4$  T and  $d = 50$  nm. The vertical axes in (d) and (e) are the same.

That the energy flux is positive can be explained as follows. Under  $B = 0$ , the surface polaritons of the InSb plate are reciprocal and so is the transmission coefficient  $\xi$ . Because  $\delta n(\omega, q_x v_d) > -\delta n(\omega, -q_x v_d)$  for  $\omega > q_x v_d$  with  $q_x > 0$ , the energy transfer of the positive  $q_x$  dominates over that of the negative  $q_x$  and the net energy flux is from the plate of the GhBN to that of the InSb. The argument can be confirmed by the energy transmission function  $\mathcal{Z}$  in Fig. 1(d) and the spectrum  $h(\omega)$  in Fig. 1(e) at  $v_d = 0.3v_F$  and  $d = 10$  nm. The two positive peaks in the spectrum correspond to the two surface-polariton frequencies of InSb and are due to the difference between the contributions from positive and negative  $q_x$ . It can be seen from Fig. 1(c) that the energy flux decreases with increasing the separation  $d$ , which is due to the evanescent nature of the surface modes.

*Energy transfer at finite  $B$ .*— We now consider the situation where a magnetic field  $\mathbf{B} = B\hat{y}$  is applied to the magneto-optic medium. The positive and negative magnetic fields  $B$  are, respectively, defined as along the positive and negative directions of the  $y$  axis. The dispersion of the surface polaritons in the magneto-optic plate is nonreciprocal in the Voigt configuration, which is schematically explained in Fig. 2(a) for  $B > 0$ . For the  $p$ -polarized mode, the electric-field components  $\mathbf{E}$  are in the incidence plane. The electrons in the magneto-optic medium experience a velocity of  $\mathbf{v} \sim \mathbf{E} \times \mathbf{B}$  due to Lorentz force. The velocity retards and accelerates the electrons whose in-plane wave-vector components are along the positive and negative  $x$  directions, respectively. Thus, the energy and the damping of the surface polaritons with positive (negative)  $q_x$  are increased (decreased) for  $B > 0$ . This scenario is opposite for  $B < 0$ .

The surface polaritons of the InSb plate for positive and negative  $\text{Re}(q_x)$  are shown in Fig. 2(b) at  $B = 4$  T. Here,  $q_x$  is complex by taking the dissipation into account in Eq. (6). It can be seen from Fig. 2(b) that the dampings at  $\text{Re}(q_x) < 0$  are stronger than those at  $\text{Re}(q_x) > 0$ . For the case with reciprocal surface modes and photonic transmission coefficients, the en-

ergy transfer of  $\delta n(\omega, q_x v_d)$  with  $q_x v_d > 0$  dominates over that of  $\delta n(\omega, -q_x v_d)$ , which leads to the net energy flux flowing out of the GhBN plate. However, because of the nonreciprocal surface polaritons of the magneto-optic medium, the photonic transmission coefficients are different for wave vectors of  $(q_x, q_y)$  and  $(-q_x, q_y)$ . This enables to change the direction of the net energy flux by magnetic field.

Figure 2(c) shows the energy flux versus the gap separation at  $B = 4$  T (solid line) and  $B = -4$  T (dashed line) with  $v_d = 0.3v_F$ . At  $B = 4$  T, the energy flux is negative when the gap separation is larger than about 18 nm. To understand this, we show the energy transmission function in Fig. 2(d) and the energy flux spectrum  $h(\omega)$  in Fig. 2(e) at  $B = 4$  T and  $d = 50$  nm. The energies  $\hbar\omega$ , around which the energy transfer is prominent, are indicated by arrows in Figs. 2(b) and 2(d). The arrows correspond to the peaks in Fig. 2(e). The contributions from the positive and negative  $q_x$  give rise to the positive and negative peaks, respectively. It can be seen that the negative peak is broader than the two positive peaks, which originates from the nonreciprocity of the surface polaritons of InSb. Therefore, it is the increased polariton damping at negative  $q_x$  and the decreased damping at positive  $q_x$  that give rise to the negative energy flux at  $B = 4$  T and  $d \gtrsim 18$  nm. The energy flux is positive at  $B = 4$  T and  $d \lesssim 18$  nm since the nonreciprocity of the effective photonic temperature in graphene increases with increasing the magnitude of wave vector  $q_x$ . Thus, the interplay between the nonreciprocal effective temperature and the nonreciprocal surface modes determines the net energy-transfer direction. For  $B = -4$  T, the surface-polariton broadening of InSb occurs at positive  $q_x$  so that the synergy from the nonreciprocal effects of the effective temperature and the surface polaritons gives rise to the positive energy flux in Fig. 2(c).

The behaviors of the energy flux versus the magnetic field  $B$  at  $d = 50$  nm are displayed in Fig. 3. The energy flux of  $v_d = 0.3v_F$  vanishes at certain magnetic fields which are denoted as  $B_-$ ,  $B_1$  and  $B_2$ . Under a small magnetic field

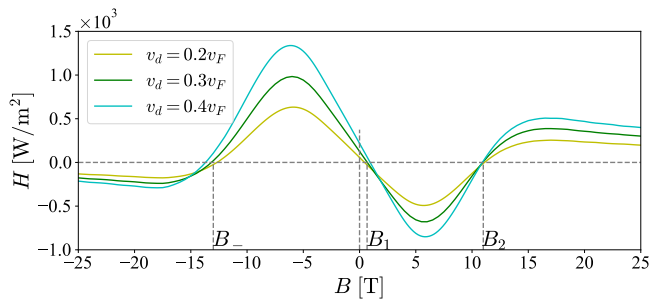


FIG. 3. Energy flux  $H$  versus magnetic field  $B$  at different drift velocities  $v_d$  with  $d = 50$  nm and  $T_1 = T_2 = 300$  K.

( $0 < B < B_1$ ), the nonreciprocity of the surface modes of InSb is weak so that the energy transfer direction is determined by the nonreciprocity of the effective photonic temperature in graphene and is from the GhBN to the InSb. With increasing the magnetic field, the energy flux becomes negative for  $B_1 < B < B_2$  and then positive for  $B > B_2$ . For  $B \leq 0$ , with increasing the magnetic-field magnitude, the energy flux first increases and then decreases and finally becomes negative for  $B < B_-$ . The negativity (positivity) of the energy flux for  $B_1 < B < B_2$  ( $B_- < B < 0$ ) can be explained in the same way as that for  $B = 4$  T ( $B = -4$  T) in Fig. 2(c).

The phenomena that the energy fluxes become positive and negative for  $B > B_2$  and  $B < B_-$ , respectively, can be explained similarly. When the magnetic field is strong enough, the surface polaritons in InSb become highly nonreciprocal. For  $B > B_2$ , the surface waves at  $q_x < 0$  are strongly damped so that their contribution to the energy transfer is suppressed. Therefore, the contribution of energy transfer from  $q_x > 0$  dominates over that from  $q_x < 0$  above a certain magnetic field, which leads to the net energy flow from the GhBN plate to the InSb one. For  $B < B_-$ , the contribution from  $q_x > 0$  is dominant and this leads to the negative energy flux.

In above, we have discussed the scenario where the in-plane magnetic field is perpendicular to the electric current. With the magnetic field being parallel to the electric current, the surface polaritons of the magneto-optic medium are reciprocal along the direction of the electric current. In this case, the net energy transfer is from the graphene to the magneto-optic medium since there is no interplay between the nonreciprocal effective photonic temperature and the nonreciprocal surface modes.

*Thermoelectric effect.*— The phenomena discussed in this work have an interesting implication of thermoelectric effect. We consider the same setup with a temperature bias between the two slabs and there is no external electric current applied to the graphene. With a magnetic field in the magneto-optic medium along the  $y$  axis, the heat-transfer rates at momenta  $q_x$  and  $-q_x$  are different so that the electrons in graphene of momenta  $q_x$  and  $-q_x$  have different kinetic energy [see Fig. 4]. When the impurity scattering in graphene is weak, this kinetic-energy difference induces an electric current along the  $x$  direction in graphene due to its high electron mobility. The

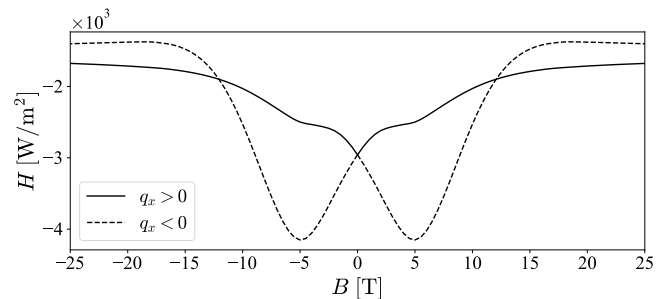


FIG. 4. Energy flux  $H$  versus magnetic field  $B$  with  $d = 50$  nm. Here, the contributions to the energy flux from positive  $q_x$  (solid line) and negative  $q_x$  (dashed line) are plotted separately. The plates have different temperatures with  $T_1 = 300$  K and  $T_2 = 330$  K, and the electric current is not externally applied. The negativity of the energy flux indicates that the heat flows from the InSb plate to that of the GhBN.

magnitude and direction of the induced electric current can be controlled by the magnetic field. To this end, the near-field thermoelectric effect can be achieved. The thermoelectric effect is analogous to the near-field propulsion force (or lateral Casimir force) in Refs. [9, 10] where the thermal energy is converted into mechanical work.

To conclude, we have studied the near-field energy transfer between graphene and magneto-optic media. The energy transfer is driven by the electric current through the graphene in the absence of a temperature difference. Its direction and magnitude can be tuned by the electric current and also the in-plane magnetic field in the magneto-optic medium. The tunability of the direction is due to the interplay between the nonreciprocal effective temperature of the graphene plasmon and the nonreciprocal surface modes of the magneto-optic medium. The energy flux can be manifested in the temperature change of the plates so that cooling or heating purposes are achieved. The findings are also relevant to near-field thermoelectric effect. Our work paves a new route towards the nanoscale energy/thermal management and harvesting using nonreciprocity.

G.T. acknowledges financial support from the Swiss National Science Foundation (SNSF) and the NCCR Quantum Science and Technology. L.Z. and J.C. acknowledge support from the National Natural Science Foundation of China (Grants No. 12074230, 11674204, 12047571), National Key R&D Program of China under Grants No. 2017YFA0304203, 1331KSC, Shanxi Province 100-Plan Talent Program. Y.Z. acknowledges support of the National Natural Science Foundation of China (Grant No. 52076056). C.T.C. acknowledges support from the Hong Kong RGC (16303119).

\* gaomin.tang@unibas.ch  
† chenjun@sxu.edu.cn

- [1] P. Ben-Abdallah, Photon thermal Hall effect, *Phys. Rev. Lett.* **116**, 084301 (2016).
- [2] L. Zhu and S. Fan, Persistent directional current at equilibrium in nonreciprocal many-body near field electromagnetic heat transfer, *Phys. Rev. Lett.* **117**, 134303 (2016).
- [3] L. Zhu, Y. Guo, and S. Fan, Theory of many-body radiative heat transfer without the constraint of reciprocity, *Phys. Rev. B* **97**, 094302 (2018).
- [4] E. Moncada-Villa, V. Fernández-Hurtado, F. J. García-Vidal, A. García-Martín, and J. C. Cuevas, Magnetic field control of near-field radiative heat transfer and the realization of highly tunable hyperbolic thermal emitters, *Phys. Rev. B* **92**, 125418 (2015).
- [5] I. Latella and P. Ben-Abdallah, Giant thermal magnetoresistance in plasmonic structures, *Phys. Rev. Lett.* **118**, 173902 (2017).
- [6] R. M. Abraham Ekeroth, P. Ben-Abdallah, J. C. Cuevas, and A. García-Martín, Anisotropic thermal magnetoresistance for an active control of radiative heat transfer, *ACS Photonics* **5**, 705 (2018).
- [7] C. Guo, B. Zhao, D. Huang, and S. Fan, Radiative thermal router based on tunable magnetic Weyl semimetals, *ACS Photonics* **7**, 3257 (2020).
- [8] A. Ott and S.-A. Biehs, Thermal rectification and spin-spin coupling of nonreciprocal localized and surface modes, *Phys. Rev. B* **101**, 155428 (2020).
- [9] D. Gelbwaser-Klimovsky, N. Graham, M. Kardar, and M. Krüger, Near field propulsion forces from nonreciprocal media, *Phys. Rev. Lett.* **126**, 170401 (2021).
- [10] C. Khandekar, S. Buddhiraju, P. R. Wilkinson, J. K. Gimzewski, A. W. Rodriguez, C. Chase, and S. Fan, Nonequilibrium Casimir effects of nonreciprocal surface waves (2021), arXiv:2106.10584.
- [11] D. S. Borgnia, T. V. Phan, and L. S. Levitov, Quasi-relativistic doppler effect and non-reciprocal plasmons in graphene (2015), arXiv:1512.09044.
- [12] B. V. Duppen, A. Tomadin, A. N. Grigorenko, and M. Polini, Current-induced birefringent absorption and non-reciprocal plasmons in graphene, *2D Materials* **3**, 015011 (2016).
- [13] T. A. Morgado and M. G. Silveirinha, Drift-induced unidirectional graphene plasmons, *ACS Photonics* **5**, 4253 (2018).
- [14] T. A. Morgado and M. G. Silveirinha, Nonlocal effects and enhanced nonreciprocity in current-driven graphene systems, *Phys. Rev. B* **102**, 075102 (2020).
- [15] M. Papaj and C. Lewandowski, Plasmonic nonreciprocity driven by band hybridization in moiré materials, *Phys. Rev. Lett.* **125**, 066801 (2020).
- [16] T. A. Morgado and M. G. Silveirinha, Negative Landau damping in bilayer graphene, *Phys. Rev. Lett.* **119**, 133901 (2017).
- [17] Y. Dong, L. Xiong, I. Y. Phinney, Z. Sun, R. Jing, A. S. McLeod, S. Zhang, S. Liu, F. L. Ruta, H. Gao, Z. Dong, R. Pan, J. H. Edgar, P. Jarillo-Herrero, L. S. Levitov, A. J. Millis, M. M. Fogler, D. A. Bandurin, and D. N. Basov, Fizeau drag in graphene plasmonics, *Nature* **594**, 513 (2021).
- [18] W. Zhao, S. Zhao, H. Li, S. Wang, S. Wang, M. I. B. Utama, S. Kahn, Y. Jiang, X. Xiao, S. Yoo, K. Watanabe, T. Taniguchi, A. Zettl, and F. Wang, Efficient Fizeau drag from Dirac electrons in monolayer graphene, *Nature* **594**, 517 (2021).
- [19] C. H. Henry and R. F. Kazarinov, Quantum noise in photonics, *Rev. Mod. Phys.* **68**, 801 (1996).
- [20] A. I. Volokitin and B. N. J. Persson, Theory of the interaction forces and the radiative heat transfer between moving bodies, *Phys. Rev. B* **78**, 155437 (2008).
- [21] A. I. Volokitin and B. N. J. Persson, Quantum friction, *Phys. Rev. Lett.* **106**, 094502 (2011).
- [22] A. I. Volokitin and B. N. J. Persson, Near-field radiative heat transfer between closely spaced graphene and amorphous SiO<sub>2</sub>, *Phys. Rev. B* **83**, 241407 (2011).
- [23] J. Peng and J.-S. Wang, Current-induced heat transfer in double-layer graphene, arXiv:1805.09493.
- [24] P. Wurfel, The chemical potential of radiation, *J. Phys. C: Solid State Phys.* **15**, 3967 (1982).
- [25] K. Chen, P. Santhanam, S. Sandhu, L. Zhu, and S. Fan, Heat-flux control and solid-state cooling by regulating chemical potential of photons in near-field electromagnetic heat transfer, *Phys. Rev. B* **91**, 134301 (2015).
- [26] K. Chen, P. Santhanam, and S. Fan, Near-field enhanced negative luminescent refrigeration, *Phys. Rev. Applied* **6**, 024014 (2016).
- [27] L. Zhu, A. Fiorino, D. Thompson, R. Mittapally, E. Meyhofer, and P. Reddy, Near-field photonic cooling through control of the chemical potential of photons, *Nature* **566**, 239 (2019).
- [28] S. M. Rytov, *Theory of Electrical Fluctuation and Thermal Radiation* (Academy of Science of USSR, Moscow, 1953).
- [29] D. Polder and M. Van Hove, Theory of radiative heat transfer between closely spaced bodies, *Phys. Rev. B* **4**, 3303 (1971).
- [30] C. Hargreaves, Anomalous radiative transfer between closely spaced bodies, *Phys. Lett. A* **30**, 491 (1969).
- [31] J. B. Pendry, Radiative exchange of heat between nanostructures, *J. Phys.: Condens. Matter* **11**, 6621 (1999).
- [32] K. Joulain, J.-P. Mulet, F. Marquier, R. Carminati, and J.-J. Greffet, Surface electromagnetic waves thermally excited: Radiative heat transfer, coherence properties and Casimir forces revisited in the near field, *Surf. Sci. Rep.* **57**, 59 (2005).
- [33] A. I. Volokitin and B. N. J. Persson, Near-field radiative heat transfer and noncontact friction, *Rev. Mod. Phys.* **79**, 1291 (2007).
- [34] B. Song, A. Fiorino, E. Meyhofer, and P. Reddy, Near-field radiative thermal transport: From theory to experiment, *AIP Adv.* **5**, 053503 (2015).
- [35] X. Liu, L. Wang, and Z. M. Zhang, Near-field thermal radiation: Recent progress and outlook, *Nanoscale and Microscale Thermophys. Eng.* **19**, 98 (2015).
- [36] J. C. Cuevas and F. J. García-Vidal, Radiative heat transfer, *ACS Photonics* **5**, 3896 (2018).
- [37] S.-A. Biehs, R. Messina, P. S. Venkataram, A. W. Rodriguez, J. C. Cuevas, and P. Ben-Abdallah, Near-field radiative heat transfer in many-body systems, *Rev. Mod. Phys.* **93**, 025009 (2021).
- [38] See Supplemental Material for details of the numerical calculation.
- [39] B. Hu, Y. Zhang, and Q. J. Wang, Surface magneto plasmons and their applications in the infrared frequencies, *Nanophotonics* **4**, 383 (2015).
- [40] E. Liu, Y. Sun, N. Kumar, L. Muechler, A. Sun, L. Jiao, S.-Y. Yang, D. Liu, A. Liang, Q. Xu, J. Kroder, V. Süß, H. Borrmann, C. Shekhar, Z. Wang, C. Xi, W. Wang, W. Schnelle, S. Wirth, Y. Chen, S. T. B. Goennenwein, and C. Felser, Giant anomalous Hall effect in a ferromagnetic kagome-lattice semimetal, *Nat. Phys.* **14**, 1125 (2018).
- [41] R. Singha, S. Roy, A. Pariari, B. Satpati, and P. Mandal, Magnetotransport properties and giant anomalous Hall angle in the half-Heusler compound TbPtBi, *Phys. Rev. B* **99**, 035110 (2019).
- [42] P. Li, J. Koo, W. Ning, J. Li, L. Miao, L. Min, Y. Zhu, Y. Wang, N. Alem, C.-X. Liu, Z. Mao, and B. Yan, Giant room temperature anomalous Hall effect and tunable topology in a ferromagnetic topological semimetal Co<sub>2</sub>MnAl, *Nat. Commun.* **11**, 3476

- (2020).
- [43] J. Hofmann and S. Das Sarma, Surface plasmon polaritons in topological Weyl semimetals, *Phys. Rev. B* **93**, 241402 (2016).
  - [44] O. V. Kotov and Y. E. Lozovik, Giant tunable nonreciprocity of light in Weyl semimetals, *Phys. Rev. B* **98**, 195446 (2018).
  - [45] B. Zhao, C. Guo, C. A. C. Garcia, P. Narang, and S. Fan, Axion-field-enabled nonreciprocal thermal radiation in Weyl semimetals, *Nano Lett.* **20**, 1923 (2020).
  - [46] Y. Tsurimaki, X. Qian, S. Pajovic, F. Han, M. Li, and G. Chen, Large nonreciprocal absorption and emission of radiation in type-I Weyl semimetals with time reversal symmetry breaking, *Phys. Rev. B* **101**, 165426 (2020).
  - [47] S. Pajovic, Y. Tsurimaki, X. Qian, and G. Chen, Intrinsic nonreciprocal reflection and violation of Kirchhoff's law of radiation in planar type-I magnetic Weyl semimetal surfaces, *Phys. Rev. B* **102**, 165417 (2020).
  - [48] G. Tang, J. Chen, and L. Zhang, Twist-induced control of near-field heat radiation between magnetic Weyl semimetals, *ACS Photonics* **8**, 443 (2021).
  - [49] D. Svintsov and V. Ryzhii, Comment on "Negative Landau damping in bilayer graphene", *Phys. Rev. Lett.* **123**, 219401 (2019).
  - [50] T. Zhu, M. Antezza, and J.-S. Wang, Dynamical polarizability of graphene with spatial dispersion, *Phys. Rev. B* **103**, 125421 (2021).
  - [51] T. A. Morgado and M. G. Silveirinha, Morgado and Silveirinha reply:, *Phys. Rev. Lett.* **123**, 219402 (2019).
  - [52] A. Kumar, T. Low, K. H. Fung, P. Avouris, and N. X. Fang, Tunable light-matter interaction and the role of hyperbolicity in graphene-hBN system, *Nano Lett.* **15**, 3172 (2015).
  - [53] B. Zhao and Z. M. Zhang, Enhanced photon tunneling by surface plasmon-phonon polaritons in graphene/hBN heterostructures, *J. Heat Transfer* **139**, 022701 (2016).
  - [54] E. D. Palik, R. Kaplan, R. W. Gammon, H. Kaplan, R. F. Wallis, and J. J. Quinn, Coupled surface magnetoplasmon-optic-phonon polariton modes on InSb, *Phys. Rev. B* **13**, 2497 (1976).
  - [55] K. W. Chiu and J. J. Quinn, Magneto-plasma surface waves in solids, *Il Nuovo Cimento B (1971-1996)* **10**, 1 (1972).

## Supplemental Material for “Near-field energy transfer between graphene and magneto-optic media”

### Graphene-covered hBN

In the presence of an electric current along the  $x$  axis, the polarization function of a bare graphene sheet at angular frequency  $\omega$  and in-plane wave vector  $\mathbf{q} = (q_x, q_y)$  is expressed as [23, 49]

$$\Pi(\omega, q_x, q_y) = \frac{\mu(T)}{(\pi\hbar v_F)^2} \int_0^{2\pi} d\theta \frac{1}{(1 - \cos\theta v_d/v_F)^2} \times \frac{q_x(\cos\theta - v_d/v_F) + q_y \sin\theta}{(\hbar\omega + i\gamma_g)/(\hbar v_F) - q_x \cos\theta - q_y \sin\theta}, \quad (7)$$

with  $\mu(T) = 2k_B T \ln[2 \cosh(\frac{\mu_g}{2k_B T})]$ . Here,  $T$  is the temperature,  $\mu_g$  the chemical potential,  $\gamma_g$  the damping parameter, and  $v_d$  the drift velocity. The Fermi velocity is  $v_F = 10^6$  m/s. The sheet conductivity is given by

$$\sigma_g(\omega, q_x, q_y) = \frac{i e^2 \omega}{q^2} \Pi(\omega, q_x, q_y), \quad (8)$$

with  $q^2 = q_x^2 + q_y^2$ . In the absence of the electric current ( $v_d = 0$ ) and in the long-wavelength limit, i.e.,  $q \rightarrow 0$ , we can recover the Drude conductivity with intraband contribution [50],

$$\sigma_{\text{intra}}(\omega) = \frac{i\omega}{(\omega + i\gamma_g/\hbar)^2} \frac{2e^2 k_B T}{\pi\hbar^2} \ln \left[ 2 \cosh \left( \frac{\mu_g}{2k_B T} \right) \right]. \quad (9)$$

Figure 5 shows the real part of the graphene conductivity  $\text{Re}(\sigma_g)$  for different  $\mathbf{q} = (q_x, 0)$  with the electric current along the  $x$  axis. One can observe that  $\text{Re}(\sigma_g)$  becomes negative for frequencies below around  $q_x v_d$ . This negative conductivity region can lead to the optical gain and negative Landau damping which were discussed in bilayer graphene [14, 16]. Here, we choose the model in Ref. [49], which was generalized to the case of an arbitrary in-plane wave vector [23], to describe the polarization function. In Ref. [51], it has been shown that the presence of the negative  $\text{Re}(\sigma_g)$  region can be obtained using different models given in Refs. [11, 12, 16, 49].

We now consider the reflection coefficient at the interface between air and graphene-covered hexagonal boron nitride (GhBN). The dielectric tensor of hexagonal boron nitride (hBN) with the optical axis along the  $x$  axis is [52]

$$\bar{\epsilon}_{\text{hBN}}(\omega) = \begin{bmatrix} \epsilon_{\perp} & 0 & 0 \\ 0 & \epsilon_{\perp} & 0 \\ 0 & 0 & \epsilon_{\parallel} \end{bmatrix}, \quad (10)$$

where

$$\epsilon_m = \epsilon_{\infty, m} \left( 1 + \frac{\omega_{\text{LO}, m}^2 - \omega_{\text{TO}, m}^2}{\omega_{\text{TO}, m}^2 - \omega^2 - i\gamma_m \omega} \right) \quad (11)$$

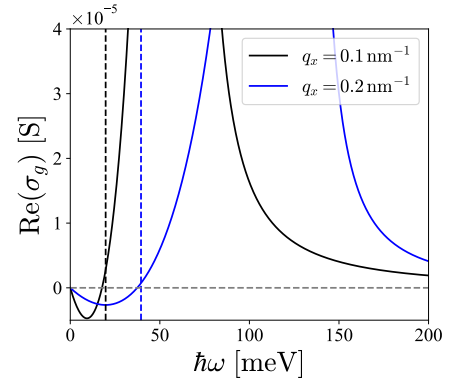


FIG. 5. Real part of the graphene surface conductivity  $\text{Re}(\sigma_g)$  versus  $\hbar\omega$  for different  $q_x$  and  $q_y = 0$  with electric current along the  $x$  axis. Here,  $\mu_g = 0.1$  eV,  $\gamma_g = 3.7$  meV,  $v_d = 0.3v_F$ , and  $T = 300$  K. The vertical dashed lines denote  $\omega = q_x v_d$  for the corresponding  $q_x$ .

	$\epsilon_{\infty, m}$	$\omega_{\text{TO}, m}$ (rad/s)	$\omega_{\text{LO}, m}$ (rad/s)	$\gamma_m$ (rad/s)
$m = \perp$	4.87	$2.58 \times 10^{14}$	$3.03 \times 10^{14}$	$9.42 \times 10^{11}$
$m = \parallel$	2.95	$1.47 \times 10^{14}$	$1.56 \times 10^{14}$	$7.54 \times 10^{11}$

TABLE I. Parameters for calculating the dielectric tensor of hBN.

with  $m = \perp, \parallel$ . The relevant parameters are given in Table I. The reflection coefficients are given by [16, 53]

$$r^p = \frac{\beta_0 \epsilon_{\perp} - \beta_1 + \beta_0 \beta_1 \sigma_g / \omega}{\beta_0 \epsilon_{\perp} + \beta_1 + \beta_0 \beta_1 \sigma_g / \omega}, \quad (12)$$

$$r^s = \frac{\beta_0 - \beta_1' - \sigma_g \omega}{\beta_0 + \beta_1' + \sigma_g \omega}, \quad (13)$$

where the superscripts  $p$  and  $s$ , respectively, denote the  $p$ - and  $s$ -polarized modes. Here, the amplitude of the out-of-plane wave vector in air is given by  $\beta_0 = \sqrt{k_0^2 - q^2}$ , and those in the GhBN are  $\beta_1 = \sqrt{\epsilon_{\perp} k_0^2 - \epsilon_{\perp} q^2 / \epsilon_{\parallel}}$  and  $\beta_1' = \sqrt{\epsilon_{\perp} k_0^2 - q^2}$  with  $k_0 = \omega/c$ . The reflection-coefficient matrix at the interface between air and the GhBN is written as

$$R_1 = \begin{bmatrix} r^p & 0 \\ 0 & r^s \end{bmatrix}. \quad (14)$$

The dispersion of the surface plasmon polariton of the GhBN is expressed as

$$\beta_0 \epsilon_{\perp} + \beta_g + \beta_0 \beta_g \sigma_g / \omega = 0. \quad (15)$$

### Magneto-optic medium

We consider magneto-optic medium InSb where the magnetic field  $B$  is applied along the  $y$  direction. The dielectric tensor is expressed as [54]

$$\bar{\epsilon}_{\text{MO}}(\omega) = \begin{bmatrix} \epsilon_d & 0 & i\epsilon_a \\ 0 & \epsilon_p & 0 \\ -i\epsilon_a & 0 & \epsilon_d \end{bmatrix}, \quad (16)$$

where

$$\epsilon_d = \epsilon_\infty \left[ 1 + \frac{\omega_L^2 - \omega_T^2}{\omega_T^2 - \omega^2 - i\Gamma\omega} + \frac{\omega_p^2(\omega + i\gamma)}{\omega[\omega_c^2 - (\omega + i\gamma)^2]} \right], \quad (17)$$

$$\epsilon_p = \epsilon_\infty \left[ 1 + \frac{\omega_L^2 - \omega_T^2}{\omega_T^2 - \omega^2 - i\Gamma\omega} - \frac{\omega_p^2}{\omega(\omega + i\gamma)} \right], \quad (18)$$

$$\epsilon_a = \frac{\epsilon_\infty \omega_p^2 \omega_c}{\omega[(\omega + i\gamma)^2 - \omega_c^2]}. \quad (19)$$

The parameters are taken from Refs. [4, 54] with the high-frequency dielectric constant  $\epsilon_\infty = 15.7$ , the longitudinal optical phonon frequency  $\omega_L = 3.62 \times 10^{13}$  rad/s, the transverse optical phonon frequency  $\omega_T = 3.39 \times 10^{13}$  rad/s, the phonon damping constant  $\Gamma = 5.65 \times 10^{11}$  rad/s, the free-carrier damping constant  $\gamma = 3.39 \times 10^{12}$  rad/s, the plasma frequency  $\omega_p = 3.14 \times 10^{13}$  rad/s, and the cyclotron frequency  $\omega_c = 8.02 \times 10^{12}$  rad/s for  $B = 1$  T.

The dispersion of the surface polaritons in the Voigt config-

uration can be obtained as [39, 48, 55]

$$\epsilon_v \beta_0 + \beta_2 - i\epsilon_a q_x / \epsilon_d = 0, \quad (20)$$

with the Voigt dielectric function  $\epsilon_v = \epsilon_d - \epsilon_a^2 / \epsilon_d$ . The out-of-plane wave vectors in air and in the magneto-optic medium are, respectively, given by  $\beta_0 = \sqrt{k_0^2 - q_x^2}$  and  $\beta_2 = \sqrt{\epsilon_v k_0^2 - q_x^2}$ . One can solve Eq. (20) to get

$$\begin{aligned} & [(\epsilon_a^2 / \epsilon_d^2 - \epsilon_v^2 - 1)^2 - 4\epsilon_v^2] q_x^4 \\ & + 2(\epsilon_v^2 + \epsilon_v)(\epsilon_a^2 / \epsilon_d^2 - \epsilon_v^2 - 1 + 2\epsilon_v) k_0^2 q_x^2 \\ & + (\epsilon_v^2 - \epsilon_v)^2 k_0^4 = 0. \end{aligned} \quad (21)$$

In the absence of a magnetic field, the dispersion becomes  $q_x = \pm \sqrt{\epsilon_d / (\epsilon_d + 1)} k_0$ . The reflection-coefficient matrix at the interface between air and the magneto-optic medium is written as

$$R_2 = \begin{bmatrix} r^{pp} & r^{ps} \\ r^{sp} & r^{ss} \end{bmatrix}, \quad (22)$$

and the calculation details can be found in the Supporting Information of Ref. [48].